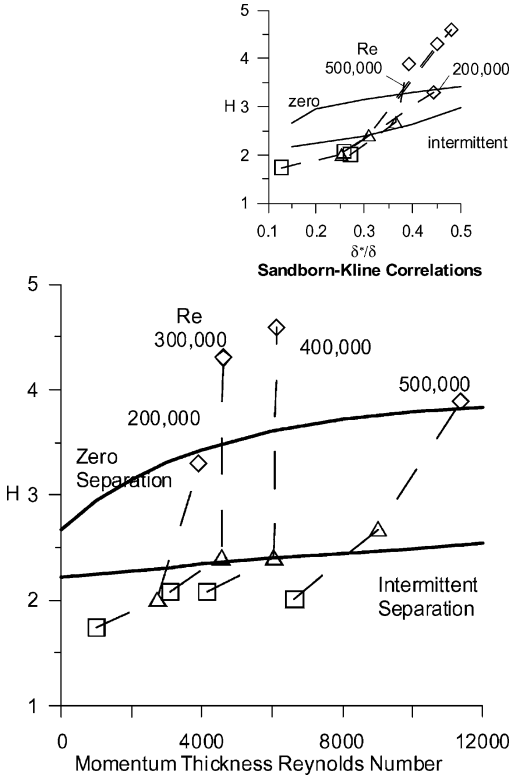

Fig. 4 Comparison of the velocity profile parameters with the separation correlations.

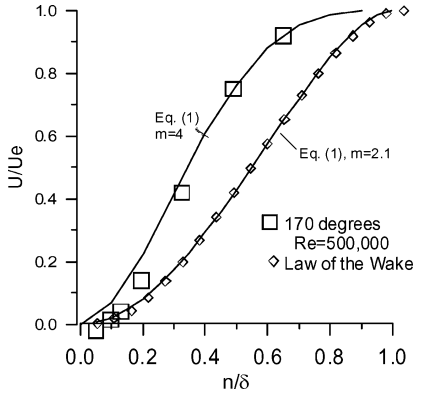

Fig. 5 Mean velocity distributions compared with Eq. (1).

The point of zero-mean surface shear stress separation, $\overline{\tau_w} = 0$, is more of academic interest, although it plays an important role in the development of skin-friction relations[4] and empirical velocity profile representation.

The Sandborn–Kline[5] $\overline{\tau_w} = 0$ correlation was obtained by employing an empirical laminar velocity separation profile,[6]

$$U/U_e = 1 + (1 - y/\delta)^m [m \ln(1 - y/\delta) - 1] \qquad (1)$$

Figure 5 shows a comparison of the TAD velocity profile at 170 deg and $Re = 5 \times 10^5$ with Eq. (1) for the case $m = 4$. Equation (1) is also compared with the 170-deg, $Re = 2 \times 10^5$ data in Fig. 2. It was assumed that the normal coordinate n was equivalent to y. The profile (Fig. 5) is beyond the point of $\overline{\tau_w} = 0$; however, the agreement with Eq. (1) for the outer region of the profile $\overline{\tau_w} = 0$ is reasonable. The tabulated law of the wake function,[7] which is found to be one unique case of Eq. (1) for $m = 2.1$, is also shown in Fig. 5. The value of δ for the law of the wake was taken at the point where $U/U_e = 0.995$, which is consistent with the requirements of the measured profiles.[4] Equation (1) can be employed for a wide range of flows and is not limited to large aerodynamic flows.

Conclusions

The velocity distribution in a complex, small radius of curvature, TAD shear flow was shown to follow closely the separation model developed for canonical, two-dimensional, large-Reynolds-number, turbulent boundary layers. The TAD flow produces a very thin shear layer along the inner surface of the initial 90 deg of the turn. Beyond 90 deg, the inner wall shear layer thickens and develops to the start of separation by approximately 150 deg around the turn. The shear layer velocity shape parameters are found to develop through the separation region as predicted by the Sandborn–Kline separation model.

The mean velocity distributions in the region of zero-mean surface shear stress separation were shown to agree with equivalent laminar separation profiles.

References

[1]Sandborn, V. A., and Shin, J. C., "Water Flow Measurements in a 180 Degree Turn-Around-Duct," NASA CR NAS8-36354, 1989.

[2]Shin, J. C., "Experiments on Turbulent Shear Flow in a Turn-Around-Duct," Ph.D. Dissertation, Dept. of Civil Engineering, Colorado State Univ., Fort Collins, CO, Feb. 1990.

[3]Simpson, R. L., "Turbulent Boundary Layer Separation," *Annual Review of Fluid Mechanics*, Vol. 21, 1989, pp. 205–234.

[4]Sandborn, V. A., "Reynolds-Number Correlation for Separation of Turbulent Boundary Layers," *AIAA Journal*, Vol. 41, No. 4, 2003, pp. 744–747.

[5]Sandborn, V. A., and Kline, S. J., "Flow Models in Boundary Layer Stall Inception," *Journal of Basic Engineering*, Ser. D, Vol. 83, No. 3, 1961, pp. 317–327.

[6]Sandborn, V. A., "Equation for the Mean Velocity Distribution of Boundary Layers," NASA Memo 2-5-59E, Feb. 1959.

[7]Coles, D., "The Law of the Wake in the Turbulent Boundary Layer," *Journal of Fluid Mechanics*, Vol. 1, Pt. 2, 1954, pp. 191–226.

A. Plotkin
Associate Editor

Dynamic Motion of Rotating Bunsen Flame Tip in Microgravity

H. Gotoda* and T. Ueda†
Keio University, Yokohama 223-8522, Japan
and
R. K. Cheng‡
Lawrence Berkeley National Laboratory, Berkeley, California 94720

Introduction

MANY combustion phenomena are sensitive to natural convection, and there has been extensive microgravity combustion research on droplet combustion, solid material combustion, or gaseous combustion to elucidate the contributions of buoyancy.[1–3] These studies are mostly performed in drop towers, parabolic aircraft flights, and surrounding rockets. In a Bunsen flame formed under normal gravity, buoyancy-induced instability, that is, flame

Received 17 May 2003; revision received 19 December 2003; accepted for publication 23 January 2004.

*Research Associate, School of Science for Open and Environmental Systems, 3-14-1 Hiyoshi, Kohoku-ku, Kanagawa.

†Professor, School of Science for Open and Environmental Systems, 3-14-1 Hiyoshi, Kohoku-ku, Kanagawa; ueda@mech.keio.ac.jp. Member AIAA.

‡Senior Scientist, Environmental Energy Technologies Division; RKCheng@lbl.gov. Senior Member AIAA.

flickering, is commonly observed at the flame tip[4] and is of fundamental importance to combustion instability issues. This flickering motion has a distinct characteristic frequency ($\approx 10 \sim 20$ Hz) and is induced by the unstable interface motion between the hot products and the surrounding air.[5,6] More recently, experiments that utilized drop towers and parabolic flights have been conducted to study buoyancy effects on the wrinkling of flame configurations[7,8] and the periodic variations in flame stretch with nonunity Lewis number effect (see Ref. 9).

Flame motion with local structure of a turbulent flame based on the flamelet regime is often seen in swirling flows, subject to buoyancy effects. With respect to an experimental investigation on a flame instability generated by the combined effects of the swirling motion, buoyancy force, and Lewis number, a rotating burner that spins on its central axis produces one of the most fundamental flame configurations. Flame motions on the rotating burner at various velocity, stoichiometry, and rotation rates have been investigated with or without the Lewis number effect in normal gravity (see Refs. 10–13).

We have also conducted normal gravity experiments of flame tip motion on a rotating Bunsen burner using CH_4–air and C_3H_8–air mixtures.[14] The results showed that, at low rotation rate, the shape of conical flame remains relatively unchanged. Beyond a critical rotation rate, the flame shape deviates from the conical shape. The evolution of flame distortions with burner rotation rate is different for flames with the Lewis number $Le > 1$ and $Le \leq 1$. For $Le \leq 1$, the conical flame becomes an eccentric flame with increasing swirl number and eventually forms a tilted flame. On the other hand, for $Le > 1$, an oscillating flame is formed with its flame tip switching back and forth between a conical shape and a buckled, that is, flattened or dimpled tip, shape. We have concluded that the oscillating flame is induced by the combination of buoyancy force, centrifugal force, and Lewis number effect (see Refs. 15 and 16). As both flow velocity and burner rotation rate increase, the oscillating flame becomes more unstable, showing that the flame tip behaves quasi periodically and nonperiodically, that is, deterministic chaotic motion.[17] These investigations indicate that the order or disorder flame motions are functions of flow velocity and burner rotation rate. The primary interest of our study is to elucidate how the buoyancy force can affect the order and disorder flame motions in swirling combustion. To investigate the buoyancy effect quantitatively, microgravity experiments are essential. The objective of this Note is then to investigate the effect of buoyancy on the periodic and nonperiodic oscillating flame motion as functions of flow velocity and burner rotation rate, using a rotating Bunsen burner system. Characterization of these flame motions would also provide insight to understand swirling combustion instability in the space environment.

Experimental Apparatus and Method

The rotating burner system shown in Fig. 1 is the same as that used in our previous works.[16,17] Fuel CH_4 is premixed with air in the mixing chamber, and the mixture flows through a diffuser, fine damping screens, a nozzle, and a burner tube. The diameter of the burner tube D_0 is 12 mm. A short honeycomb is installed in the burner tube to give rigid-body rotation of the CH_4–air mixtures.[10,11] The burner tube is vertically supported by bearings and connected by a pulley-belt system to a dc motor. As reported in our previous studies,[14] the flame shape and flame motion depend on the Lewis number, and the oscillating flame is formed when the Lewis number Le is larger than unity, that is, a rich CH_4–air mixture and lean C_3H_8–air mixture. In the present study, a rich CH_4–air mixture at the equivalence ratio $\phi = 1.43$ was used with the velocity $U = 0.6$ and 1.1 m/s. These are the conditions where we found typical periodic oscillating flame and nonperiodic oscillating flames in normal gravity. Here, U is the mean axial flow velocity of the mixture from the straight tube (equal to volume flow rate divided by cross-sectional area of the straight tube). The rotation rate of burner tube N is varied up to 2800 rpm (46.7 s^{-1}). The Reynolds number Re based on the burner tube diameter is 449 for $U = 0.6$ m/s and 748 for $U = 1.1$ m/s. To normalize the flow rotation, a swirl number S is introduced as a function of rotational speed and mean flow velocity as follows;

$$S = \frac{G_\theta}{G_x R} = \frac{2\pi \int_0^R \rho u v_\theta r^2 \, \mathrm{d}r}{2\pi R \int_0^R \rho \left(u^2 - v_\theta^2/2\right) r \, \mathrm{d}r} = \frac{2U\omega R}{4U^2 - (\omega R)^2}$$

where G_θ is the axial flux of the swirl momentum, G_x the axial flux of the linear momentum, r the radial distance, R the radius of the straight tube, u the axial velocity, v_θ the tangential velocity, $\omega (= \pi N/30)$ the angular velocity of the burner tube, and N the rotation rate (revolutions per minute) of the burner tube.

The microgravity experiments were conducted at the drop-tower of Micro-Gravity Laboratory in Japan (MGLAB) with the free-fall distance of 150 m. The microgravity level is 10^{-5} g, and the duration of the microgravity environment is 4.5 s. Details of this facility

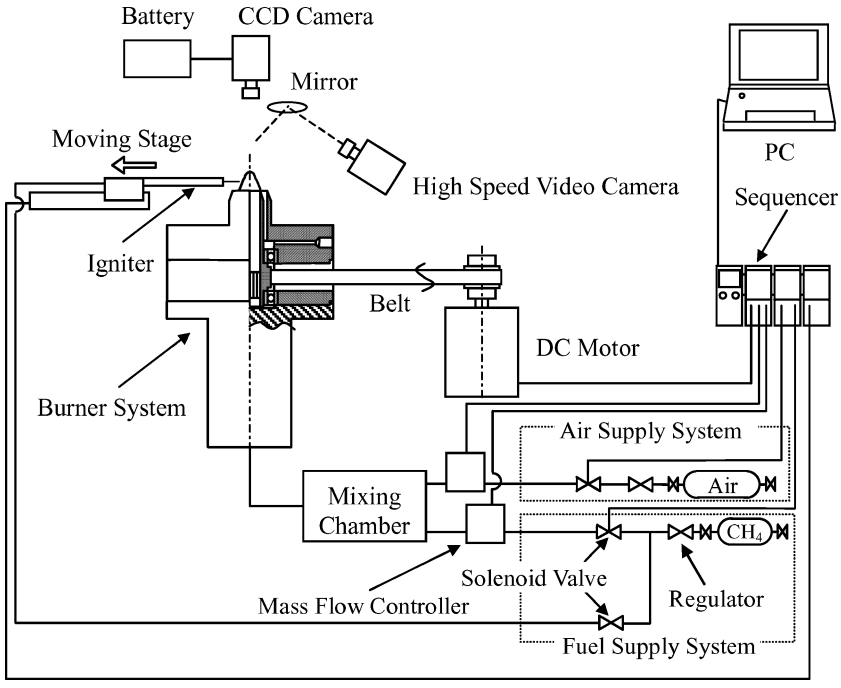

Fig. 1 Experimental apparatus.

are described in Ref. 18. As shown in Fig. 1, the rotating Bunsen burner, the igniter, mixing chambers, mass-flow controllers (Kofloc, Model 3910 Series), solenoid valves (SMC, VXZ Series), a charge-coupled device (CCD) video camera, and high-speed video camera (NAC Memrecam Ci) are included in the compact integrated module for the drop tower. The steel frame module, with a base diameter of 720 mm and height of 830 mm, is fit in the MGLAB drop capsule with an outer diameter of 900 mm and a height of 2280 mm. The support equipment, such as a gravity sensor, temperature sensor, and a pressure gauge, is also contained in the MGLAB drop capsule. Before the free fall, rich CH_4–air flame was ignited in normal gravity, followed by the initiation of burner rotation. The capsule was released for the free fall when the flame reached a stable state. The motion of rotating flames under microgravity environment was recorded with the CCD video camera of 30 frames/s and high-speed video camera of 500 frames/s.

Results and Discussion

As reported previously,[17] when both the jet velocity and the burner rotation rate are increased, the periodic oscillation mode cannot be sustained and it transits to the nonperiodic oscillation mode, that is, deterministic chaos mode, in normal gravity. To provide insight into the question on whether or not the buoyancy effect becomes irrelevant to the onset of the nonperiodic oscillation mode, we compare rotating flames with $U = 1.1$ m/s in normal gravity ($+1\ g$) and in microgravity as shown in Fig. 2 as a function of swirl number S. In $+1\ g$, the nonperiodic oscillating flame is observed in the range of $0.78 < S < 0.94$. In particular, the nonperiodic oscillating flame with most significant variation in flame curvature is formed when $S = 0.85$. The nonperiodic oscillating flame is also observed in microgravity, but the onset of nonperiodic flame motions is shifted to the lower swirl number range ($0.68 < S < 0.82$). In the microgravity environment, where the ascending buoyancy force vanishes, the centrifugal force becomes a primary factor in determining flame shape. As a result, the flame shape in microgravity becomes broader in the radial direction compared to that of the shape at $+1\ g$.

For the $S = 0.78$ flame in microgravity, a series of images taken by a CCD video camera with shutter speed 1/30 s is shown in Fig. 3. Despite no changes in the shape of the outer diffusion flame, the five images show quite complicated nonperiodic oscillating flame shape with rapid deformation. It indicates that the nonperiodic oscillations are formed without buoyancy-induced instability. However, the magnitudes of the flame tip motion on the centerline at $S = 0.78$ is supposed to be slightly lower than the $+1\ g$ case ($S = 0.85$). This indicates that the buoyancy force affects the flame motion in the case of $U = 1.1$ m/s.

Consecutive high-speed video images with shutter speed 1/500 s for $S = 0.78$ in microgravity are shown in Fig. 4. Although they are not cross-sectional images, the flame front with slight conical-shape or buckled shape are prominently shown. Furthermore, the inflection points of flame shape are noticeable even in microgravity. This indicates the nonperiodic oscillating flame with inflection point is formed by an increase in a hydrodynamic perturbation, which is inherently included in the flow with an increase in both jet inertial force and the centrifugal force. Because the images taken in microgravity are integrated, the quantitative analysis to elucidate whether or not the nonperiodic oscillation is chaotic has not been done in the present study. If the cross-sectional tomographic images are obtained in microgravity, the chaotic motion in the microgravity condition can be quantified by applying the analytical method based on deterministic chaos theory proposed by the authors.[17]

Figure 5 shows the map of flame shape as a function of S. In the case of $U = 0.6$ m/s in microgravity, the flame tip ceases to oscillate, but the flame tip at $S = 0.86$ gradually moves downward from slightly cone shape to buckled shape, whereas the outer diffusion flame does not show any movement. This indicates that there is no stable point and the stable conical flame suddenly transits to stable plateau flame at some critical value of $S (S = 0.86)$. This brings out an interesting fact on the stability of swirling microgravity flames in that there is a discontinuity variation between the regimes of stable conical flame and the plateau flame. When U is 1.1 m/s, a domain of the nonperiodic oscillating flame is found between the stable conical flame and plateau flame. This indicates that the increase in both flow velocity and burner rotation rate increases the hydrodynamic perturbation that induces the nonperiodic oscillation in both microgravity and $+1\ g$.

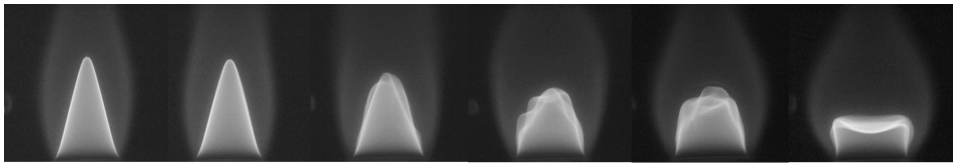

a)

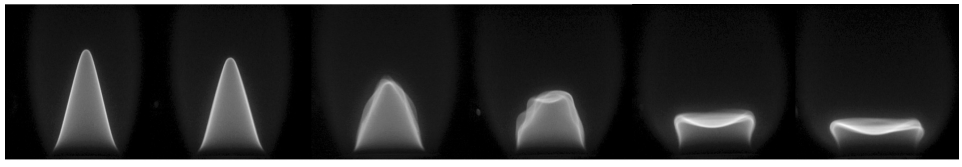

b)

Fig. 2 Rotating flames with $U = 1.1$ m/s in a) normal gravity ($+1\ g$) and b) microgravity as a function of swirl number S.

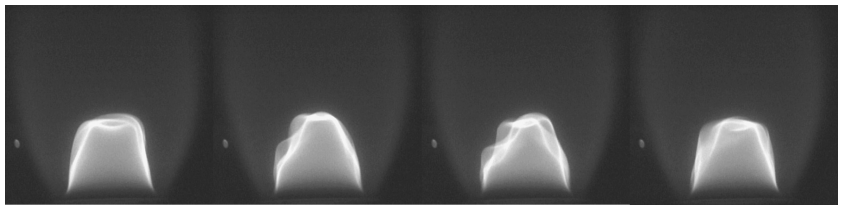

Fig. 3 Time variations in the flame motion with $S = 0.85$ in microgravity.

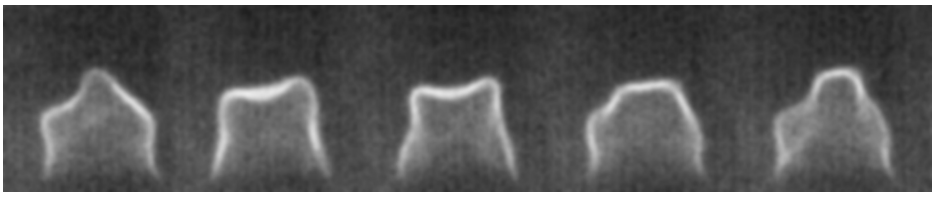

Fig. 4 High-speed video images of flame motion with $S = 0.85$ in microgravity.

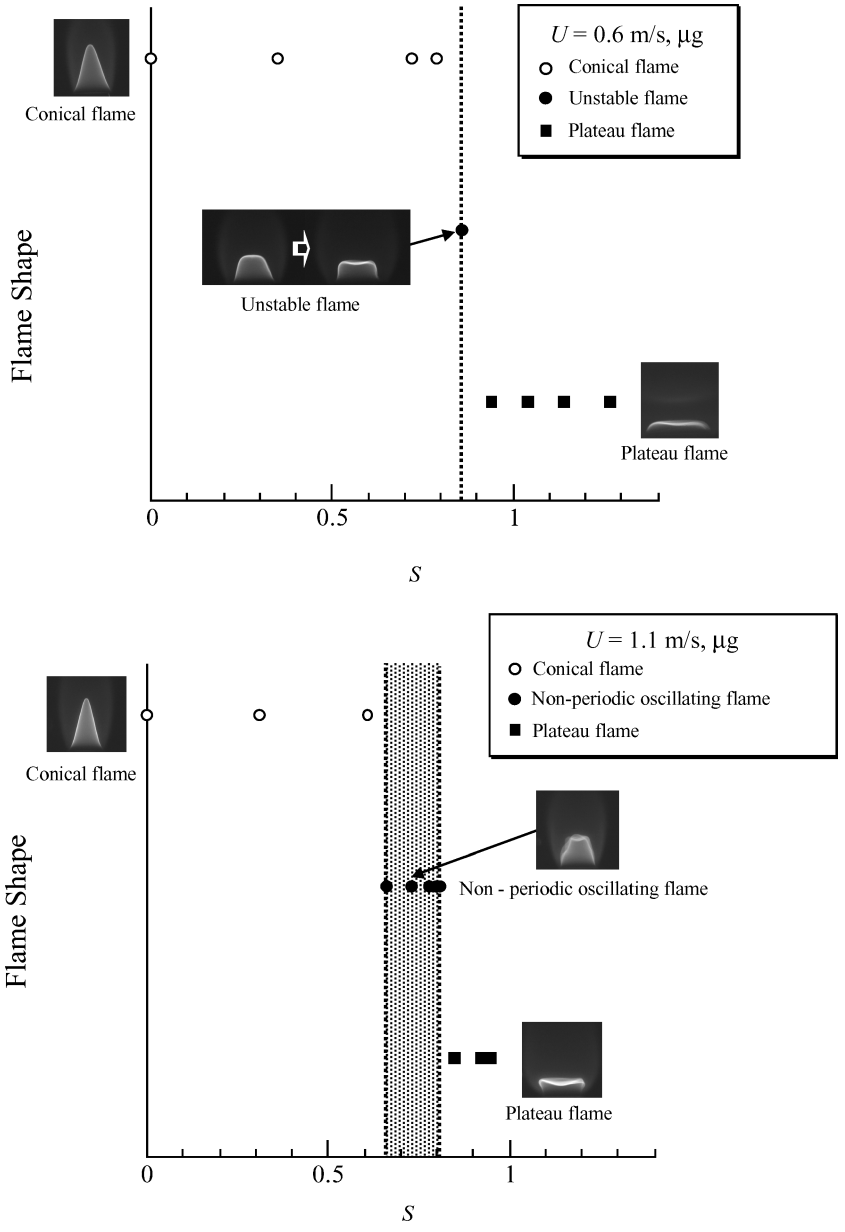

Fig. 5 Stability map of microgravity flame shapes as a function of *S*.

From these results, buoyancy effect on the dynamics of unsteady flame with burner rotation can be summarized as follows. The $+1$ g periodic oscillating flame formed in $U = 0.6$ m/s is due to the buoyancy-driven instability, whereas the nonperiodic oscillating flame in $U = 1.1$ m/s is induced by the hydrodynamic effect due to the combination of inertial jet force and centrifugal force. This shows that, under the condition of $Le > 1$, the hydrodynamic instability due to the combination of the jet inertial force and centrifugal force plays an important role in switching from periodic mode to nonperiodic mode.

Summary

Dynamic motion of a premixed Bunsen flame with burner rotation has been investigated experimentally in normal gravity ($+1$ g) and microgravity. Rotating CH_4–air flames (equivalence ratio $\phi = 1.43$) with mean flow velocities of $U = 0.6$ and 1.1 m/s have been studied for swirl number of 0–1.6.

In the microgravity condition where the ascending buoyancy force vanishes, the centrifugal force as well as jet inertial force becomes predominant in determining flame shape variations. Accordingly, the flame shape becomes broader toward the radial direction

compared to that of the $+1$ g case. When U is 0.6 m/s, the periodic oscillation of the flame tip in $+1$ g ceases to oscillate in microgravity. On the other hand, when $U = 1.1$ m/s, the flame motion becomes nonperiodic even in the microgravity condition. These results indicate that, the $+1$ g periodic oscillating flame at $U = 0.6$ m/s is induced by the buoyancy instability, whereas the nonperiodic oscillating flame at $U = 1.1$ m/s is due to the combined effect generated by both the jet inertial force and centrifugal force. That is, under the condition of $Le > 1$, the hydrodynamic instability due to the combination of the jet inertial force and centrifugal force plays an important role in switching from the periodic mode to the nonperiodic mode.

Acknowledgments

R. K. Cheng is supported by NASA Microgravity Sciences. This work has been carried out as part of a Ground-based Research Announcement for Space Utilization promoted by the Japan Space Forum. The authors thank Kazuyuki Maeda for useful comments and help in the microgravity experiments.

References

[1]Law, C. K., and Faeth, G. M., "Opportunities and Challenges of Combustion in Microgravity," *Progress in Energy and Combustion Science*, Vol. 20, 1994, pp. 65–113.

[2]Kono, M., Ito, K., Niioka, T., Kadota, T., and Sato, J., "Current State of Combustion Research in Microgravity," *Proceedings of the Combustion Institute*, Vol. 26, 1996, pp. 1189–1199.

[3]Ronney, P. D., "Understanding Combustion Processes Through Microgravity Research," *Proceedings of the Combustion Institute*, Vol. 26, 1995, pp. 2485–2506.

[4]Durox, D., Baillot, F., Scoufflaire, P., and Prud'homme, R., "Some Effects of Gravity on the Behavior of Premixed Flames," *Combustion and Flame*, Vol. 82, 1990, pp. 66–74.

[5]Kostiuk, L. W., and Cheng, R. K., "Imaging of Premixed Flames in Microgravity," *Experiments in Fluids*, Vol. 18, 1994, pp. 59–68.

[6]Koustik, L. W., and Cheng, R. K., "The Coupling of Conical Wrinkled Laminar Flames with Gravity," *Combustion and Flame*, Vol. 103, 1995, pp. 27–40.

[7]Bedat, B., and Cheng, R. K., "Effects of Buoyancy on Premixed Flame Stabilization," *Combustion and Flame*, Vol. 107, 1996, pp. 13–26.

[8]Cheng, R. K., Bedat, B., and Koustik, L. W., "Effects of Buoyancy on Lean Premixed V-Flames Part I: Laminar and Turbulent Flame Structures," *Combustion and Flame*, Vol. 116, 1999, pp. 360–375.

[9]Sinibaldi, J. O., Mueller, C. J., Tulkki, A. E., and Driscoll, J. F., "Suppression of Flame Wrinkling by Buoyancy: The Baroclinic Stabilization Mechanism," *AIAA Journal*, Vol. 36, No. 8, 1998, pp. 1432–1438.

[10]Sheu, W. J., Sohrab, S. H., and Sivashinsky, G. I., "Effect of Rotation on Bunsen Flame," *Combustion and Flame*, Vol. 79, 1990, pp. 190–198.

[11]Cha, J. M., and Sohrab, S. H., "Stabilization of Premixed Flames on Rotating Bunsen Burners," *Combustion and Flame*, Vol. 106, 1996, pp. 467–477.

[12]Ishizuka, S., "Characteristics of Tubular Flame," *Progress in Energy and Combustion Science*, Vol. 19, 1993, pp. 187–226.

[13]Sakai, Y., and Ishizuka, S., "The Phenomena of Flame Propagation in a Rotating Tube," *Proceedings of the Combustion Institute*, Vol. 26, 1996, pp. 847–853.

[14]Ueda, T., Kato, T., Matsuo, A., and Mizomoto, M., "Effect of Burner Rotation on the Flame Shape of Laminar Premixed Bunsen Flame," *2nd ASPACC on Combustion*, Australia/New Zealand, Chinese, Chinese Taipei, Japan, and Korean Secs. of the Combustion Inst., 1999, pp. 218–220.

[15]Gotoda, H., and Ueda, T., "Characteristic of Flame Tip Oscillation of a Bunsen Type Premixed Flame with Burner Rotation," *Transactions of the JSME*, Vol. 67, No. 658, 2001, pp. 1529–1535 (in Japanese).

[16]Gotoda, H., Maeda, K., Ueda, T., and Cheng, R. K., "Periodic Motion of Bunsen Flame Tip with Burner Rotation," *Combustion and Flame*, Vol. 134, 2003, pp. 67–79.

[17]Gotoda, H., and Ueda, T., "Transition from Periodic to Non-Periodic Oscillation of a Bunsen Type Premixed Flame with Burner Rotation," *Proceedings of the Combustion Institute*, Vol. 29, 2002, pp. 1503–1509.

[18]Asano, S., and Tokuo, T., "Introduction of MGLAB Drop Experiment Facilities," *Space Forum*, Vol. 6, 2000, pp. 411–416.

R. Lucht
Associate Editor

Vortex Shedding from Rectangular Plates

Alexander Yakhot*
Ben-Gurion University of the Negev, 84105 Beersheva, Israel
Nikolai Nikitin†
Moscow State University, 119899, Moscow, Russia
and
Heping Liu‡
Ben-Gurion University of the Negev, 84105 Beersheva, Israel

Introduction

VORTEX excitation from rectangular elongated plates when the length parallel to the flow is much greater than the height perpendicular to the flow has been investigated experimentally by Nakamara and Nakashima[1] and Nakamura et al.[2] They concluded that vortex shedding from elongated flat plates with square leading and trailing edges is dominated by the impinging shear layer instability, when a single separated shear layer can be unstable in the presence of a sharp downstream corner.[3] Recently, Hourigan et al.[4] considered the trailing-edge shedding to be a powerful mechanism leading to self-sustained oscillations. They found that the trailing-edge shedding plays an important role in the stepwise behavior of the Strouhal number with increasing a chord-thickness ratio, which is a subject of this Note.

Discussion

Transition in vortex shedding from the von Kármán type to the impinging shear layer instability has been observed when the Reynolds number was increased from 200 to 300 (Ref. 1). Experimental data show that on short plates ($c/t < 3$, c/t being the chord-thickness ratio) the flow separates at the leading-edge corner and the shear layers interact directly, without reattaching to the plate's surface, thus, forming a regular vortex street. On longer plates ($c/t > 3$), the shear layers are reattached upstream of the trailing edge and form a separation bubble that grows and may divide, depending on the chord-thickness ratio (c/t): $m = 1$ (one bubble) for $c/t = 3$–5, $m = 2$ (two bubbles) for $c/t = 6$–8, and $m = 3$ (three bubbles) for $c/t = 9$–12. These bubbles are convected toward the trailing edge (Fig. 1). The flow patterns reveal that the leading-edge separation bubble was nearly steady. For Reynolds numbers $Re > 300$, experimental results show that the Strouhal number $Sr(c)$, based on the chord length, increases stepwise with c/t increasing from 3 to 12, namely,

$$Sr(c) = fc/U = 0.55\,m \tag{1}$$

where f and U are the vortex shedding frequency and the freestream velocity, respectively, and m is the number of vortices (bubbles).

Vortex shedding from elongated rectangular plates has been investigated numerically in Refs. 4–6. In the present Note, we used a new numerical approach, which is based on an immersed-boundary

Received 10 September 2003; accepted for publication 4 March 2004.

*Associate Professor, Pearlstone Center for Aeronautical Engineering Studies, Department of Mechanical Engineering.

†Senior Scientist, Institute of Mechanics, 1 Michurinski prospekt.

‡Postdoctoral Student, Department of Mechanical Engineering.